Evidence for New Enantiospecific Interaction Force in Chiral Biomolecules

Yael Kapon
the Hebrew University of Jerusalem
Abhijit Saha
Indian Institute of Chemical Biology
Tal Duanias-Assaf
The Hebrew University
Thijs Stuyver
The Hebrew University
Amir Ziv
The Hebrew University
Tzuriel Metzger
The Hebrew University
Shira Yochelis
The Hebrew University
Sason Shaik
The Hebrew University
Ron Naaman
Weizmann Institute of Science https://orcid.org/0000-0003-1910-366X
Meital Reches
Hebrew University of Jerusalem https://orcid.org/0000-0001-5652-9868
Yossi Paltiel (paltiel@mail.huji.ac.il)
Hebrew University of Jerusalem https://orcid.org/0000-0002-8739-9952

Article

Keywords: enantiospecific biorecognition interaction, chiral biomolecules

Posted Date: January 19th, 2021

DOI: https://doi.org/10.21203/rs.3.rs-138903/v1

Abstract

Enantiospecific biorecognition interactions are key to many biological events. Commonly, bio-affinity values, measured in these processes, are higher than those calculated by available methods. We report here the first direct measurement of the interaction force between right and left handed helical polyalanine peptides using atomic force microscope (AFM) and calculations based on a simple theoretical model. A force difference of 60pN between same and opposite enantiomer interactions is measured. Additional measurements show spin dependency and fast decay of the interaction term, consistent with spin exchange interactions. This short range enantiospecific interaction term is especially relevant in crowded biological systems. The results shed light on the importance of spin and exchange interactions in biological processes, providing explanation to the discrepancies between past calculations and experiments.

Main Text

Nature is based on chiral molecules, namely molecules that appear in two forms, enantiomers, that are mirror images of each other. Interestingly, chiral biomolecules, like proteins and sugars appear in Nature mainly as one enantiomer. The origin of “homo chirality” in Nature, was – and is – discussed very intensively in the literature[1]. However, the focus of this work is related to a more fundamental question, i.e., why did Nature preserve chirality so persistently over the many millions years of evolution? In other words, does chirality per se, independent on the specific handedness, provide properties that serve an important role in Life? The ability of biological molecules to interact selectively with each other is at the heart of all biological processes and the basis of many pharmaceutical concepts. Two important properties – related to chirality – characterize interactions in nature, i.e., very strong enantioselectivity and the relatively fast rates of very complex processes, e.g., the rate of protein folding[2-4] and the repair of damage in DNA[5].

It has been suggested that an interaction term that involves the electrons’ spin can improve the enantioselectivity in reactions of chiral molecules, due to the symmetry constraints resulting from the dispersion-induced charge reorganization, which is accompanied by transient spin polarization (see Figure 1A)[6]. However, such a spin-related interaction term has never been measured before. Herein we use atomic force spectroscopy, and measure directly the enantioselective interaction between oligopeptides of different handedness. Simple modelling of the spin related enantiospecific interaction energies shows that the spin constraint imposes directionality in the interaction.

The enantioselectivity measured here does not correspond to any of the established biorecognition mechanisms related to structural properties, like the “lock and key” model[7], induced fit and allosteric interactions[8], and neither can it be explained through differential, enantiomer-specific, long-range electrostatic interactions[9-13]. Though existing computational methods account for enantioselectivity[9-11], none is able to reproduce the high selectivity observed in the present experiments[14-16]. This suggests that

the enantioselective spin interaction is not captured properly by the theories currently employed to describe (bio)molecules. While additional research will be needed to delineate the exact scope and pervasiveness of this effect, it can be expected to alleviate some of the notable discrepancies between observed vs. computed enantiospecificity, interaction energies, and reaction rates. Furthermore, the directionality emerging from our model may help to explain the high efficiency of many complex bio-processes, such as protein folding and enzymatic reactions, since it reduces significantly the phase space the systems have to explore.

When considering bio-related chemical processes, the distribution of charges in the reacting species is of major importance. Obviously, these distributions are a direct result of the spatial positions of the charged electrons and nuclei in the molecular systems. However, next to charge, electrons also have another property, their spin, which is their angular momentum and can have two orientation values. In organic molecules, the spin is typically not coupled significantly to the molecular frame and therefore the orientation of the spin relative to this frame is not defined. Consequently, in such a case, the electron's spin direction does not affect the interaction between molecules, i.e., the exchange term of the dispersion interaction is spin-independent[17]. For chiral molecules however, this is not the case. In the last two decades it was established that when electrons are displaced in a chiral system, the rate of this displacement depends on their spin. This property was termed the Chiral Induced Spin Selectivity (CISS)[18].

In chiral systems, the spin that results from the charge displacement is strongly coupled to the molecular frame, so that spins of one type are displaced faster than the other, depending on the handedness of the molecule and the direction of motion. Charge displacement occurs whenever two chiral molecules approach each other, resulting in the formation of induced electric dipoles (see Figure 1A). Consequently, the emergence of these dipoles implies that at each electric pole, there is at least a fraction of an unpaired electron, i.e., spin polarization is intrinsically associated with the electric dipole formation in chiral molecules. The concept of charge polarization accompanied by spin polarization was verified in experiments in which the interaction of chiral molecules with ferromagnetic substrates was probed[19,20]. Hence, when two chiral molecules interact, a spin-dependent interaction term emerges[21], which is dependent upon the relative handedness of the molecules.

Here we present experiments in which the force between chiral oligomer attached to the tip of an atomic force spectrometer (AFM) and a monolayer made from oligomers that possess either the same or opposite handedness, or oligomers that are not chiral, are monitored. The energies associate with the enantiospecific interactions are larger by more than a factor five compared to the thermal energies at room temperature. This part is followed by model calculations that show the role of the spin exchange interaction and its effect on the interaction energies and their angle-dependent distribution

Previous work[20] has shown that exchange interactions can be probed using modified atomic force spectroscopy (AFS). AFS is widely used to examine biological interactions and functions[22] and is used for the study of binding and unbinding of proteins[23,24]. This study utilizes the above method to probe

spin exchange interactions between helical (hence chiral) peptides and demonstrate the relation between enantiomer-selectivity and spin. A chemically modified standard gold coated AFM cantilever was used. The functionalized cantilever is used to generate a distance dependent force curve based on short-ranged spin exchange interaction. The gold AFM tip was functionalized with polyethylene glycol (PEG), 60 nm long, bound to a helical peptide, L-AHPA, where AHPA is Alpha Helix Polyalanine (AHPA) [HS-PEG-NH-AAAAKAAAAKAAAAKAAAAKAAAAKAAAAKAAAAK-COOH] (see Figure 1C, 1D). The AFM-tip was functionalized in such a way that the peptide's carboxyl group is facing the substrate (see methods section for details). The PEG acts as a spacer to reduce non-specific interactions and the whole system is immersed in ethanol to eliminate capillary forces. The measured samples consist of self-assembled monolayers of the same helical polypeptide adsorbed on a gold substrate. The adsorption process ensures a peptide alignment such that the carboxylic group is facing up, so that there are no covalent bonds possible between the oligopeptide peptide on the AFM tip and the one adsorbed on the substrate. Over a thousand curves of force vs. distance were measured, which were subsequently examined manually. Following previous studies[20,25,26], only curves that showed a clear pulling event (see in supplementary Figure S1), were further analyzed as single molecule rapture events. A worm-like chain (WLC) model was then fitted on the specific interaction's pulling event and the pulling force was retrieved. The mean pulling force (MPF) was calculated by averaging over the selected pulling forces.

The force between the same and different enantiomers is presented in Figure 2. Right or left-handed helical oligopeptides (L-AHPA or D-AHPA respectively) were measured when adsorbed on the gold substrate. As control experiments, we measured a monolayer of a non-chiral - 12-mercaptododecanoic acid with a comparable length and an equivalent carboxylic head group facing up. The mean pulling force of the molecules is shown in Figure 2A. A force difference of between the interaction of the homochiral pair of oligopeptides (L-AHPA monolayer – L-AHPA) and the interaction of the heterochiral pair (D-AHPA monolayer – L-AHPA adsorbed AFM tip) is obtained. The interaction's energy is retrieved by integrating the force distance curve over the pulling event. An average energy difference of about is measured (Supplementary Figure S2).

A sum of two Gaussians is fitted to the force distributions presented in Figure 2B to highlight the concept of multiple forces that are acting between the molecules (quality of fit is shown in Figure S4). This is done to differentiate between the long-range interactions and the short-range spin exchange interactions[20]. We attribute the first Gaussian, at low forces, to non-specific interactions that are the same for all samples (i.e., Coulomb and dispersive forces). The second, at higher forces, is attributed to the spin-dependent exchange interaction and is different for homo and hetero chiral interactions, i.e., this force is stronger between same enantiomers (L-L) than opposite enantiomers (L-D). As a control experiment, we checked non chiral molecules as well. The MPF between the L-AHPA adsorbed on the tip and non-chiral control was lower than the force for both enantiomers. This effect will be discussed below. It is interesting to note that the MPF of the plain gold sample is lower than the MPF of the chiral L-L interaction. At first sight, this may be surprising since the interaction between a gold substrate and a

carboxylic group has a covalent character, but it can be explained by the gold being coated with organic contamination[27,28].

To verify that the difference in the binding of the two enantiomers results from the spin effect, a sample of gold substrate with adsorbed L-AHPA monolayer was tested (Figure 3 A1). Due to the sulfur-gold bond, the sample becomes paramagnetic[29-32]. By adding an external, out-of-plane, magnetic field, the spin injection into the chiral monolayer can be controlled. The same functionalized tip, as described above, was used and a constant applied magnetic field perpendicular to the surface was applied during the measurement (see Figure 3A1). The results are presented in Figure 3 A2 and Figure 3 A3. The MPF difference between up and down magnetizations is (Figure 3A2). These results support the notion that the interaction's strength is spin dependent. A clear difference is also seen in the force distributions histograms (Figure 3 A3).

The effect of the substrate magnetization on the force measured in the case of chiral molecules can also be a result of more efficient charge penetration from the substrate into the chiral molecule, when the injected charge has the preferred spin for the given handedness[33]. This charge transport from the substrate increases the spin density at the interaction between the molecule attached to the tip and the adsorbed molecule. To evaluate this effect, we investigated the interaction of a tip coated with achiral molecule with oligopeptide adsorbed on magnetized substrates (Supplementary Figure S5). In this case the difference in the force measured for the two directions of magnetization is within the noise range of the system. Thus, the main difference in force under opposite magnetic field is a result of spin-dependent exchange interactions.

We have shown so far that spin is affecting the bio-recognition pulling force. To relate the results to exchange interactions only, and to differentiate them from mechanical and structural related forces, we probed the interaction range. The spin-exchange interaction is characterized by overlap of wavefunctions and is therefore short-ranged. In a previous study, the decay length of the spin-dependent interaction was determined to be about 0.7 nm[34]. To probe the range of the effect observed in the present study, a layer of a non-chiral amino-acid (glycine), 0.4 nm long, was added to the respective helical peptide monolayers (L/D-AHPA), which are 2 nm high. The adsorption of the glycine was done following a protocol reported in the literature[35,36], and the experimental layout and of the monolayer with glycine is presented in Figure 3 B1. The samples were measured with the same functionalized AFM cantilever as before. The results are presented in Figure 3 B2 and 3 B3. The force histograms in Figure 3 B3 are fitted with a sum of two Gaussians to differentiate between the long-range interactions and the short-range spin exchange interactions. A difference in the MPF of was measured suggesting the effect is still apparent but weaker then without the a-chiral separation. An additional verification of the range of the force was performed with samples having a thicker bi-layer of glycine (0.8 nm) and the results are presented in the inset of Figure 3 B3. In the case of a sample in which the chiral molecules are separated by 0.8 nm, the difference in the force between the enantiomers has completely disappeared, suggesting a length dependent of the force as expected in the case of spin-related interactions[34]. These results also suggest that the

penetration of the helical peptide into the monolayer is also short-ranged, otherwise the structural differences would become apparent in the interaction.

To obtain an insight into the observed spin-dependent exchange interaction and its relation to enantio-selective interaction between biomolecules, we developed a “toy model” that – despite its simplicity – captures the essential physics in a phenomenological manner. Since – as mentioned above – none of the currently available electronic structure programs enable a proper description of the transient spin polarization, we opted to mimic this phenomenon through inclusion of so-called “spin polarization-sources” (vide infra) within a Valence Bond (VB) framework[37]. In our toy model, the two chiral helices are represented as 2 two-site systems, i.e., two H2-like molecules. For the resulting four-site system, 6 (covalent) VB determinants can be defined, corresponding to the different distributions of 2 α- and 2 β-electrons in 4 orbitals (see Supplementary Figure S7). In the dissociation limit, i.e., in the limit of infinite separation between the two molecules, the spins will not interact with each other. To phenomenologically enforce (dispersion-induced) spin polarization, we add a “spin polarization-source” to each of the molecules (Supplementary Figure S8A). These spin polarization-sources are single sites with a predefined/fixed spin which induce spin polarization in the adjacent molecules by increasing/decreasing the energy of the respective VB determinants. As can be seen from Supplementary Figure S8B and S8C, placing the two sources with an opposing spin leads to spin polarization of the same sign in both molecules; placing them with a parallel spin leads to spin polarization of the opposite sign in both molecules. Note that the distance between the source and the actual molecule is an arbitrary parameter which sets the extent of induced spin-polarization; in the calculations performed, a distance of 0.1 nm was selected, which results in net spins of approximately 0.33e on each of the individual sites of the molecules in the dissociation limit.

As expected, in the dissociation limit, the spin polarized wavefunctions obtained for the two spin-polarization-source alignments are degenerate in energy. When the spacing between the two molecules is reduced however, this degeneracy is broken: at a distance of 2-3 Å between the two molecules, the spin interaction starts to become significant.

Next to the (spin-dependent) exchange term, a Lennard-Jones potential with parameters σ=0.16 nm and ε=3.0 kcal/mol was added to the model to collectively account for all the spin-independent interaction terms. The resulting potential energy profile is shown in Figure 4A for the case of collinear approach of the two spin polarized species. The energy one samples with the AFM measurements corresponds to the difference between the bottom of the well in each potential (namely for the two spin configurations, parallel and antiparallel spins). It should be clear that the toy model provides qualitative result that are consistent with the experimental measurements. Figure 4B shows the angle and distance dependence of the energy difference for the two spin configurations. This plot reveals a clear preference for a collinear configuration due to the spin exchange interaction.

The preference for a narrow range of approach angles emerging from our model can be expected to be relevant to many complex biological processes, since it may reduce the phase space that a system has to

explore before reacting, thus enhancing reaction rates. As such this relatively subtle, yet probably ubiquitous, effect may be responsible for the remarkable speed of bio-recognition effects in protein folding and in searching DNA by enzymes.

To summarize, three experiments using chiral atomic force microscopy were presented. The first, directly measured the interaction force difference between same and opposite enantiomers. The second and third experiments show interactions between helical peptides and present two main characteristics of the exchange interaction, its spin dependency and its short range (. The third experiment also suggests that the peptide adsorbed on the tip of the AFM does not penetrate more than into the monolayer. Our findings suggest that spin-dependent exchange interaction may play a pivotal role in biorecognition processes. The energy scale for L-AHPA L-AHPA interactions is on the order of . When the chiral molecules interact, symmetry constrains that arise from the chirality create a different spin distribution for homochiral and heterochiral interaction. A toy model for the enantiomer-specific interaction shows that the interaction is controlled by the exchange interaction of electron spin pairs and exhibits a significant radial dependence. The experimental results and the model calculations suggest an additional interaction term, not taken into account so far, that may explain enhanced enantiospecificity and rates for various important processes occurring in Biology. The new interaction term introduces short range force that is especially relevant to biological systems, where the interacting systems are typically in crowded environment.

Methods

Materials:

Fmoc-L-Ala-OH, Fmoc-L-Lys (Boc)-OH and Fmoc-L-Lys (Boc)-Wang resin [0.343 meq/gm and 100-200 mesh] were purchased from Chem-Impex. NHS-PEG-S-Trt were purchased from Iris Biotech GMBH. N, N-dimethylformamide (DMF), dichloromethane (DCM), piperidine, methanol, trifluoroacetic acid (TFA), diethyl ether, methanol (MeOH) and ethanol (EtOH) were purchased from Bio-Lab (Jerusalem, Israel). Tri isopropyl silane (TIPS), Oxyma pure, N, N-diisopropylcarbodiimide (DIC), 1,2-ethanedithiol (EDT), ninhydrin, phenol, pyridine and Fmoc-6-Ahx-OH were purchased from Sigma Aldrich.

Molecule Synthesis:

The thiol functionalized PEGylated chiral (and helical) polypeptide, Alpha Helix Polyalanine (AHPA) [HS-PEG-NH-AAAAKAAAAKAAAAKAAAAKAAAAKAAAAKAAAAK-COOH] and the thiol functionalized PEGylated non-helical reference compound [HS-PEG-NH-6-Ahx-K-COOH] were synthesized on solid phase following solid phase peptide synthesis procedure using microwave peptide synthesizer (CEM, Discover Bio). Fmoc-L-Lys (Boc)-Wang resin [0.343 meq/gm and 100-200 mesh] was used as solid support. The resin was swelled for overnight in dichloromethane (DCM) and N, N-dimethyl formamide (DMF) solvent mixture (1:1) prior the synthesis. The Fmoc deprotection was performed by 20% piperidine in DMF and coupling reaction was performed using Oxyma pure and N, N-diisopropylcarbodiimide (DIC) in DMF solvent under microwave. Fmoc-L-Ala-OH, Fmoc-L-Lys (Boc)-OH and NHS-PEG-S-Trt were used to make the chiral alpha

helix polyalanine. Fmoc-6-Ahx-OH and NHS-PEG-S-Trt were used to make the non-helical reference compound. Ninhydrin test was performed at each step of coupling and Fmoc-deprotection to check whether the reaction was completed or not.

Cleavage of molecule from the resin:

The resin was washed five times with each of the following solvents DMF, DCM, methanol and diethyl ether and kept under vacuum for 4 hours to ensure complete dryness. Cleavage cocktail containing 92.5% TFA, 2.5% TIPS, 2.5% EDT and 2.5% water was used. The molecule attached on the resin was taken with the cocktail mixture and shacked for 4 hours at room temperature. The solution was drained and poured into ice cold diethyl ether for precipitation. It was kept at -20 °C for overnight and centrifugated at 5000 rpm at 4 °C. The residue was dissolved in water and lyophilized. A white solid compound was obtained.

Tip functionalization and AFM measurements:

The solid compound was dissolved in triple distilled water to prepare 1 mM solution. The gold-tip was washed with EtOH, dried in air and incubated with the 1 mM solution of the molecule for overnight at room temperature. The tip again was washed with water to remove the non-attached molecules and dried in air. AFM measurements were performed in EtOH.

Samples preparation:

A gold substrate [Si / Cr (15nm) / Au (100nm)] was used for all samples' preparation. The substrates were cleaned by boiling (70oC) acetone and then ethanol for 10 minutes each. Then the samples were introduced into a plasma Asher system (Diener PICO UHP) for 10 minutes at 50% strength. Finally, the samples were soaked in absolute ethanol for 20 minutes and dried under nitrogen.

1st part: The plain gold substrate reference sample was cleaned as above. The L and D AHPA samples and non-chiral [12-mercaptododecanoic acid] sample were prepared by wet chemistry, dipping the gold substrates in a 1mM solution of: L-AHPA [L-AHPA-36 (1mM)] /D-AHPA [D-AHPA-36 (1mM)] / non-chiral molecule [12-mercaptododecanoic acid (1mM)] overnight. Then, rinsing in absolute ethanol and drying under hydrogen. The whole process is done under nitrogen chamber.

2nd part: L-AHPA molecules were adsorbed on a gold substrate as in the 1st part. The molecules were measured under a constant magnetic field of 3000 Gauss using an external magnet during the measurement.

3rd part: L and D AHPA samples on gold substrate were prepared as in the 1st part. The monolayers' carboxylic groups were activated by an EDC-NHS process standard protocol. Then Glycine was added to the samples for two hours. Finally, the samples were rinsed with water and dried with nitrogen. For the thicker layer of glycine, the process was repeated twice.

Force spectroscopy measurements:

Force spectroscopy curves were retrieved using JPK AFM (NanoWizard3®). A commercially available gold-coated tip was functionalized by immersing the tip for 20 min in ethanol and then by overnight adsorption of the abovementioned molecules. Over 1000 curves were taken (1500-4500 depending on the sample). Only the curves that showed a significant distinguished pulling event were taken and analyzed by the JPK data analysis software. The worm like chain (WLC) model was fitted to the pulling events to find the rupture point and pulling force (see Figure S1). The force distribution from a sample was fitted to a sum of gaussians and the mean probable force (MPF) was retrieved by averaging the pulling forces.

Declarations

Funding: Y.P. and R.N. acknowledge the support of the John Templeton Foundation and the MOS Israel. R.N. acknowledges the partial support of the ISF and of the Minerva Foundation. S. S. and T. S. are supported by the ISF grant 520/18. T.S. acknowledges the Research Foundation-Flanders (FWO) for a position as a postdoctoral research fellow (1203419N). A.S. acknowledges the support of the Shunbrun Fellowship.

Author contribution: Y. K. and A. S. performed and analyzed the experimental results. T. D. and A. Z. helped in the AFM measurements. T. M. and S. Y. helped in all the chemical aspects of the paper. T. S. did the modeling and theoretical calculations. S. S. was supervising the theoretical part of the manuscript, S. Y., M. R., R. N. and Y. P. conceived the experimental part of the work and participated in planning and analyzing the results; All authors participated in writing the manuscript. All the data are presented in the manuscript and supplementary materials.

Conflict of interests: The authors declare no conflict of interests.

References

1. Blackmond, D. G. The Origin of Biological Homochirality. *Cold Spring Harb. Perspect. Biol.* **11**, a032540 (2019).
2. Ivankov, D. N. & Finkelstein, A. V. Prediction of protein folding rates from the amino acid sequence-predicted secondary structure. *Proc. Natl. Acad. Sci.* **101**, 8942–8944 (2004).
3. Qiu, L., Pabit, S. A., Roitberg, A. E. & Hagen, S. J. Smaller and Faster: The 20-Residue Trp-Cage Protein Folds in 4 μs. *J. Am. Chem. Soc.* **124**, 12952–12953 (2002).
4. Glyakina, A. V. & Galzitskaya, O. V. How Quickly Do Proteins Fold and Unfold, and What Structural Parameters Correlate with These Values? *Biomolecules* **10**, (2020).
5. Carusillo, A. & Mussolino, C. DNA Damage: From Threat to Treatment. *Cells* **9**, 1665 (2020).
6. Kumar, A. *et al.* Chirality-induced spin polarization places symmetry constraints on biomolecular interactions. *Proc. Natl. Acad. Sci.* **114**, 2474–2478 (2017).
7. Fischer, E. Einfluss der Configuration auf die Wirkung der Enzyme. *Berichte Dtsch. Chem. Ges.* **27**, 2985–2993 (1894).

8. Schneider, H.-J. Limitations and Extensions of the Lock-and-Key Principle: Differences between Gas State, Solution and Solid State Structures. *Int. J. Mol. Sci.* **16**, 6694–6717 (2015).
9. Ramanan, R., Dubey, K. D., Wang, B., Mandal, D. & Shaik, S. Emergence of Function in P450-Proteins: A Combined Quantum Mechanical/Molecular Mechanical and Molecular Dynamics Study of the Reactive Species in the H2O2-Dependent Cytochrome P450SPα and Its Regio- and Enantioselective Hydroxylation of Fatty Acids. *J. Am. Chem. Soc.* **138**, 6786–6797 (2016).
10. Wang, Z., Danovich, D., Ramanan, R. & Shaik, S. Oriented-External Electric Fields Create Absolute Enantioselectivity in Diels-Alder Reactions: The Importance of the Molecular Dipole Moment. *J. Am. Chem. Soc.* **140**, (2018).
11. Dubey, K. D. & Shaik, S. Cytochrome P450—The Wonderful Nanomachine Revealed through Dynamic Simulations of the Catalytic Cycle. *Acc. Chem. Res.* **52**, 389–399 (2019).
12. Sheng, X., Kazemi, M., Planas, F. & Himo, F. Modeling Enzymatic Enantioselectivity using Quantum Chemical Methodology. *ACS Catal.* **10**, 6430–6449 (2020).
13. Schopf, P. & Warshel, A. Validating computer simulations of enantioselective catalysis; reproducing the large steric and entropic contributions in Candida Antarctica lipase B. *Proteins Struct. Funct. Bioinforma.* **82**, 1387–1399 (2014).
14. Goh, B. C. *et al.* Computational Methodologies for Real-Space Structural Refinement of Large Macromolecular Complexes. *Annu. Rev. Biophys.* **45**, 253–278 (2016).
15. Mortier, J. *et al.* The impact of molecular dynamics on drug design: applications for the characterization of ligand–macromolecule complexes. *Drug Discov. Today* **20**, 686–702 (2015).
16. Jing, Z. *et al.* Polarizable Force Fields for Biomolecular Simulations: Recent Advances and Applications. *Annu. Rev. Biophys.* **48**, 371–394 (2019).
17. Danovich, D. *et al.* Understanding the Nature of the CH···HC Interactions in Alkanes. *J. Chem. Theory Comput.* **9**, 1977–1991 (2013).
18. Naaman, R., Paltiel, Y. & Waldeck, D. H. Chiral molecules and the electron spin. *Nat. Rev. Chem.* **3**, 250–260 (2019).
19. Banerjee-Ghosh, K. *et al.* Separation of enantiomers by their enantiospecific interaction with achiral magnetic substrates. *Science* **360**, 1331–1334 (2018).
20. Ziv, A. *et al.* AFM-Based Spin-Exchange Microscopy Using Chiral Molecules. *Adv. Mater.* **31**, 1904206 (2019).
21. Happer, W. & Tam, A. C. Effect of rapid spin exchange on the magnetic-resonance spectrum of alkali vapors. *Phys. Rev. A* **16**, 1877–1891 (1977).
22. Bizzarri, A. R. & Cannistraro, S. The application of atomic force spectroscopy to the study of biological complexes undergoing a biorecognition process. *Chem. Soc. Rev.* **39**, 734–749 (2010).
23. Hinterdorfer, P., Baumgartner, W., Gruber, H. J., Schilcher, K. & Schindler, H. Detection and localization of individual antibody-antigen recognition events by atomic force microscopy. *Proc. Natl. Acad. Sci.* **93**, 3477–3481 (1996).

24. Hugel, T. & Seitz, M. The Study of Molecular Interactions by AFM Force Spectroscopy. *Macromol. Rapid Commun.* **22**, 989–1016 (2001).
25. Das, P., Duanias-Assaf, T. & Reches, M. Insights into the Interactions of Amino Acids and Peptides with Inorganic Materials Using Single-Molecule Force Spectroscopy. *J. Vis. Exp. JoVE* (2017) doi:10.3791/54975.
26. Razvag, Y., Gutkin, V. & Reches, M. Probing the Interaction of Individual Amino Acids with Inorganic Surfaces Using Atomic Force Spectroscopy. *Langmuir* **29**, 10102–10109 (2013).
27. Paik, W., Han, S., Shin, W. & Kim, Y. Adsorption of Carboxylic Acids on Gold by Anodic Reaction. *Langmuir* **19**, 4211–4216 (2003).
28. Miller, D. *et al.* Static SIMS studies of carboxylic acids on gold and aluminium–magnesium alloy surfaces. *Surf. Interface Anal.* **35**, 463–476 (2003).
29. Carmeli, I., Leitus, G., Naaman, R., Reich, S. & Vager, Z. Magnetism induced by the organization of self-assembled monolayers. *J. Chem. Phys.* **118**, 10372–10375 (2003).
30. Crespo, P. *et al.* Permanent Magnetism, Magnetic Anisotropy, and Hysteresis of Thiol-Capped Gold Nanoparticles. *Phys. Rev. Lett.* **93**, 087204 (2004).
31. Hernando, A., Crespo, P. & García, M. A. Origin of orbital ferromagnetism and giant magnetic anisotropy at the nanoscale. *Phys. Rev. Lett.* **96**, 057206 (2006).
32. Yamamoto, Y. *et al.* Direct observation of ferromagnetic spin polarization in gold nanoparticles. *Phys. Rev. Lett.* **93**, 116801 (2004).
33. Ghosh, S. *et al.* Effect of Chiral Molecules on the Electron's Spin Wavefunction at Interfaces. *J. Phys. Chem. Lett.* **11**, 1550–1557 (2020).
34. Metzger, T. S. *et al.* The Electron Spin as a Chiral Reagent. *Angew. Chem. Int. Ed.* **59**, 1653–1658 (2020).
35. Hermanson, G. T. *Bioconjugate Techniques*. (Elsevier, 1996).
36. Buttafoco, L. *et al.* First steps towards tissue engineering of small-diameter blood vessels: preparation of flat scaffolds of collagen and elastin by means of freeze drying. *J. Biomed. Mater. Res. B Appl. Biomater.* **77**, 357–368 (2006).
37. Shaik, S. S. & Hiberty, P. C. *A Chemist's Guide to Valence Bond Theory*. (2007).

Figures

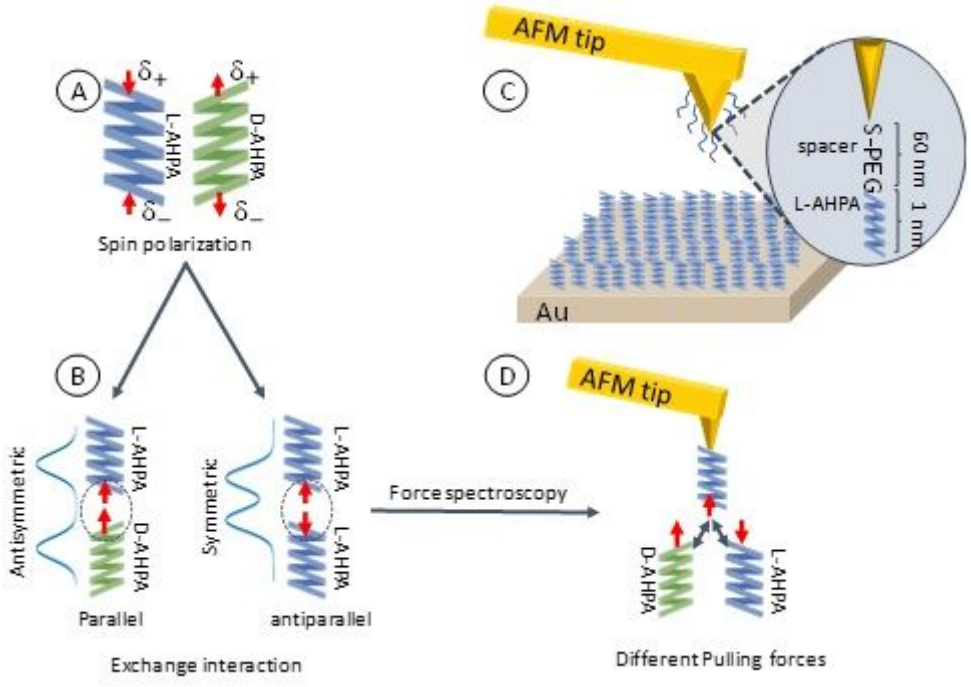

Figure 1

A scheme of the interaction induced spin polarization and the experimental set up. A) When chiral molecules interact, charge reorganization occurs and an electric dipole is created with a positive (δ+) and negative (δ-) charge. Which spin polarization (red arrows) is associated with which pole, depends on the handedness of the molecules. B) On the left- If the two interacting molecules are of opposite handedness, the two interacting spins are parallel (high spin). On the right- If the molecules are of the same handedness, the spins are opposite to each other (low spin). C) The experimental configuration that includes the AFM system and a monolayer of oligopeptides adsorbed as a self-assembled monolayer on a gold substrate. In the scheme, the interaction between the L-AHPA on the tip and a monolayer of L-AHPH on substrate is presented. D) A gold AFM tip is functionalized with L-AHPA ligands. The molecule is separated from the tip by PEG with a length of 60 nm to reduce nonspecific interactions. The system is immersed in ethanol to eliminate capillary forces. While approaching the substrate, an electric dipole is induced in both the molecule on the tip and in the monolayer, resulting in a transient charge movement. As a result of the CISS effect, there is spin polarization associated with each electric pole. At short distance, the molecule on the tip interacts with the molecule on the substrate. Due to the handedness of the interacting molecules there is a different exchange interaction for the two different enantiomers, similar to the different between interactions occurring either on a triplet or singlet potential energy surface. Therefore, when detaching the tip from the monolayer, a different pulling force is measured for the interaction of the same or opposite enantiomers.

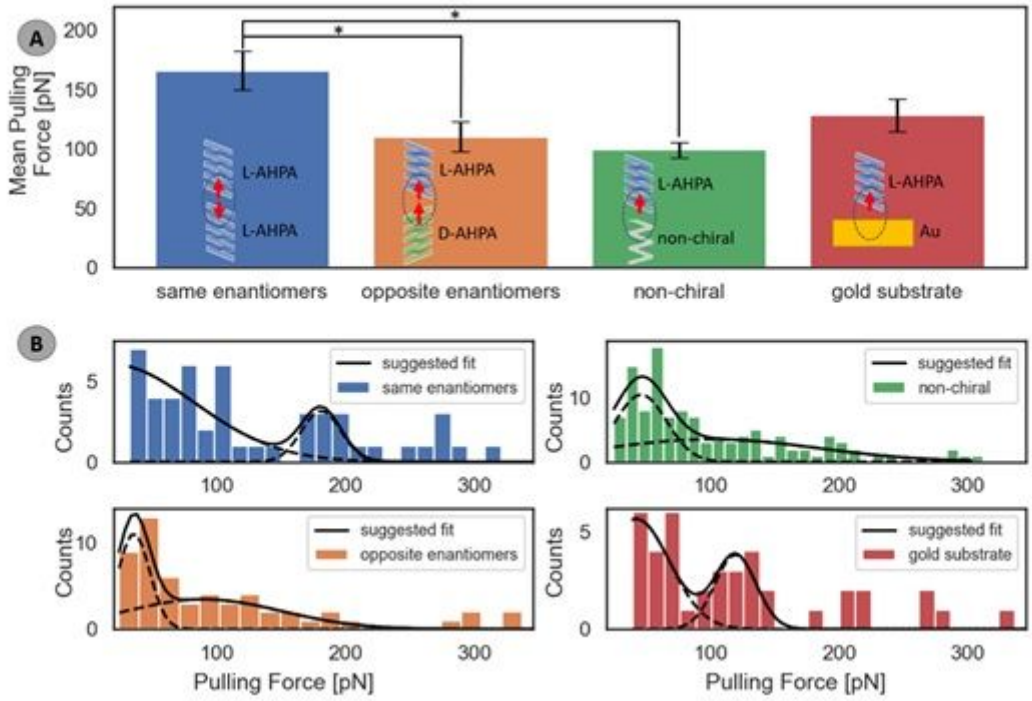

Figure 2

Force spectroscopy measurements of enantioselectivity. A) Mean pulling force (MPF) between the molecule on the tip (L-AHPA) and an AHPA monolayer adsorbed on a gold substrate. A non-chiral monolayer (mercaptododecanoic acid) as well as a clean substrate were used as a control experiment. For AHPA monolayers a difference in the MPF is measured for same (L-monolayer) or opposite (D-monolayer) enantiomer interaction. The same enantiomer interaction is stronger by 60±20 pN. B) The force distributions. The suggested fit is a sum of two Gaussians. The wide range of forces suggests multiple interactions. The dashed line displays the suggested fitted Gaussians (see also Figure S4).*statistical comparison tests (ANOVA followed by post hoc Tukey test) showed a significant difference ($p<0.01$) between the marked data sets (see SI for more information)

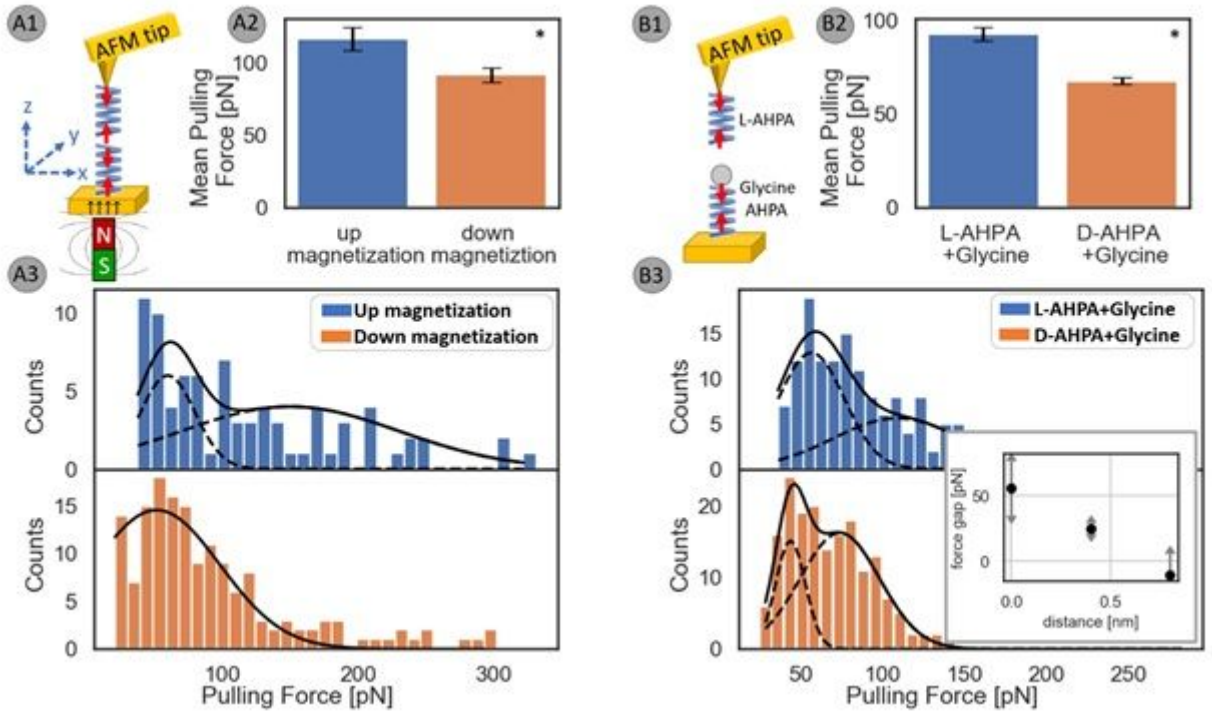

Figure 3

Force spectroscopy results under constant magnetic field. A1) Schematic of the experimental system where the force is measured under different spin injection conditions. A magnet is placed under the sample with a constant magnetic field. This changes the spin wave function, resulting in different measured pulling force. A2) Mean pulling force (MPF) between the molecule on the tip (L-AHPA) and an L-AHPA monolayer adsorbed on gold substrate under magnetic field. A difference in the MPF is measured up or down magnetization. The interaction under out of plain magnetic field is stronger by 28±9 pN demonstrating the dependence of the pulling force strength on the spin wavefunction. A3) Force distributions histograms. The suggested fit is a sum of two Gaussians. For the down magnetization, a single Gaussian was fitted for better fit. Force spectroscopy results for separated chiral monolayer. B1) Schematics of the measurement system. A glycine layer was added to an adsorbed AHPA monolayer. The glycine's carboxyl group facing up. B2) Mean pulling force (MPF) between the molecule on the tip (L-AHPA) and the monolayer. In this case smaller difference is measured in the MPF between the monolayers. To see the effect clearer, the force distributions are analyzed. B3) The force distributions. Sum of Gaussians are fitted to the distribution. The first correspond to the nonspecific interaction. The second corresponds to the exchange interaction. A different force for L and D monolayers is measured. This is the enantiospecific force. The inset displays the decay of the mean pulling force difference between L and D, for adding zero, one (Figure 3 B2), or two glycine layers (see SI Figure S6). Each glycine layer add 4Å to the thickness. *statistical comparison tests (ANOVA followed by post hoc Tukey test) showed a significant difference ($p<0.01$) between the marked data sets (see SI for more information)

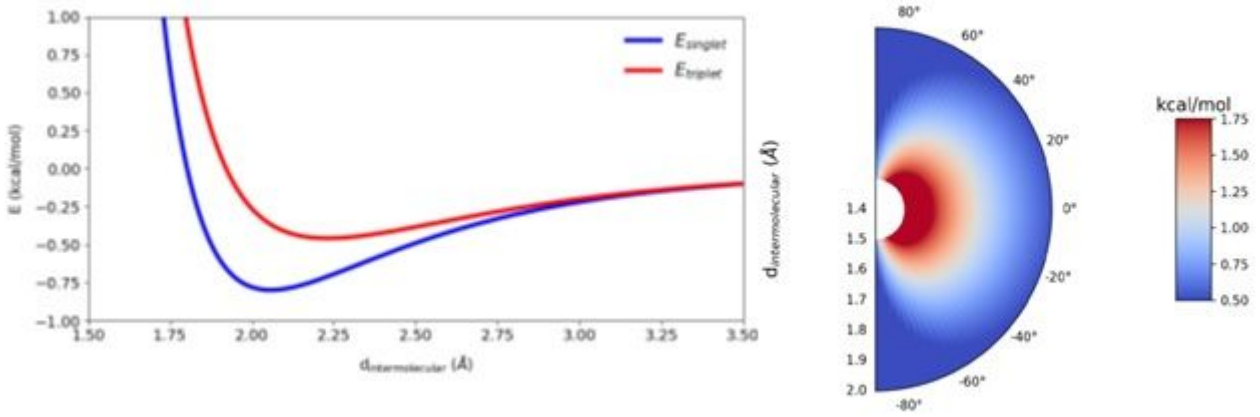

Figure 4

The results from the model calculations. A) The potential energies related to the interaction of two molecules with spin polarized either antiparallel (blue) or parallel (red) to each other. The calculation is for a collinear approach. The potentials were calculated using a spin exchange energy term to which a Lennard-Jones potential with the parameters σ=0.16 nm and ε=3.0 Kcal/mole was added. B) The difference is energy between parallel polarized spins versus antiparallel polarized spins as a function of both the distance and the angle between the two approaching species

Supplementary Files

This is a list of supplementary files associated with this preprint. Click to download.

- SIEvidenceforNewEnantiospecificInteractionForceinChiralBiomolecules1.docx